J|A|C|S
ARTICLES

Published on Web 04/01/2009

Probing Hydrophobic Interactions Using Trajectories of Amphiphilic Molecules at a Hydrophobic/Water Interface

Andrei Honciuc and Daniel K. Schwartz*

Department of Chemical and Biological Engineering, University of Colorado, Boulder, Colorado 80309

Received January 30, 2009; E-mail: daniel.schwartz@colorado.edu

Abstract: Individual molecules of fluorophore-labeled alkanoic acids with various chain lengths, BODIPY$-(CH_2)_n-$COOH (abbreviated as fl-C*n*), were observed to adsorb and move at the methylated fused silica−water interface as a function of temperature using total internal reflection fluorescence microscopy. The statistical analysis of squared-displacement distributions indicated that the molecular trajectories were consistent with a diffusive model involving two intertwined modes. The slower mode, typically responsible for <50% of the molecular diffusion time, had a diffusion coefficient of $<0.005\ \mu m^2/s$ and could not be distinguished from the *apparent* motions of immobilized molecules because of the limitations of experimental resolution. The faster mode exhibited diffusion coefficients that increased with temperature for all chain lengths, permitting an Arrhenius analysis. Both the effective activation energies and kinetic prefactors associated with the fast-mode diffusion coefficients increased systematically with chain length for fl-C2 through fl-C10; however, fl-C15 did not follow this trend but instead exhibited anomalously small values of both parameters. These observations were considered in the context of hydrophobic interactions between the adsorbate molecules and the methylated surface in the presence of water. Specifically, it was hypothesized that fl-C2, fl-C4, and fl-C10 adopted primarily extended molecular conformations on the hydrophobic surface. The increases in activation energy and entropy with chain length for these molecules are consistent with a picture of the transition state in which the molecule partially detaches from the surface and exhibits greater conformational freedom. In contrast, the small activation energy and entropy for fl-C15 are consistent with a scenario in which the surface-bound molecule adopts a compact/globular conformation with limited surface contact and conformational flexibility.

Introduction

The hydrophobic interaction is an interesting and intensely studied aspect of fundamental science, with relevance in many physicochemical processes of technological and biological importance.[1,2] Formation of supramolecular aggregates, vesicles and bilayers,[3] and protein folding[4] are direct consequences of hydrophobic interactions between nonpolar solutes in aqueous media. Protein aggregation due to interactions between exposed hydrophobic patches (and other interactions) is a significant concern for the pharmaceutical industry[5,6] and may also be implicated in certain disease states, such as amyloidosis.[7,8] Hydrophobic interactions are also the basis of biomolecular separation methods such as reversed-phase chromatography and hydrophobic interaction chromatography.[9,10]

Simplistically, the hydrophobic interaction can be regarded as the tendency of nonpolar groups to adhere in the presence of water in order to minimize their contact area with the aqueous solvent. Although it is not a bond but instead is nonspecific, the hydrophobic interaction is an order of magnitude stronger than van der Waals dispersion forces[11] in many cases of interest. In more quantitative terms, the hydrophobic free energy of hydration can be defined as the free energy change upon transfer of a hydrocarbon solute from a pure hydrocarbon phase into an aqueous phase.[12] A related phenomenon involves the association of two hydrophobic solute molecules that are hydrated as a pair.[13] The formation of micelles, vesicles, or aggregates falls between these idealized situations. Hydrophobic interaction forces and energies are determined experimentally using a variety of techniques, such as single-molecule force spectroscopy,[14] solvation data,[15] conductivity studies,[16] and direct measurement of forces acting between macroscopic hydrophobic

(1) Meyer, E. E.; Rosenberg, K. J.; Israelachvili, J. *Proc. Natl. Acad. Sci. U.S.A.* **2006**, *103*, 15739–15746.
(2) Tanford, C. *Protein Sci.* **1997**, *6*, 1358–1366.
(3) Israelachvili, J. N.; Mitchell, D. J.; Ninham, B. W. *J. Chem. Soc., Faraday Trans. 1* **1976**, *72*, 1525–1568.
(4) Dyson, H. J.; Wright, P. E.; Scheraga, H. A. *Proc. Natl. Acad. Sci. U.S.A.* **2006**, *103*, 13057–13061.
(5) Frokjaer, S.; Otzen, D. E. *Nat. Rev. Drug Discovery* **2005**, *4*, 298–306.
(6) Wang, W. *Int. J. Pharm.* **2005**, *289*, 1–30.
(7) Chiti, F.; Dobson, C. M. *Annu. Rev. Biochem.* **2006**, *75*, 333–366.
(8) Pepys, M. B. *Annu. Rev. Med.* **2006**, *57*, 223–241.
(9) Jungbauer, A. *J. Chromatogr. A* **2005**, *1065*, 3–12.
(10) Shi, Y.; Xiang, R.; Horvath, C.; Wilkins, J. A. *J. Chromatogr. A* **2004**, *1053*, 27–36.
(11) Israelachvili, J.; Pashley, R. *Nature* **1982**, *300*, 341–342.
(12) Gill, S. J.; Wadso, I. *Proc. Natl. Acad. Sci. U.S.A.* **1976**, *73*, 2955–2958.
(13) Wood, R. H.; Thompson, P. T. *Proc. Natl. Acad. Sci. U.S.A.* **1990**, *87*, 946–949.
(14) Ray, C.; Brown, J. R.; Akhremitchev, B. B. *J. Phys. Chem. B* **2006**, *110*, 17578–17583.
(15) Reynolds, J. A.; Gilbert, D. B.; Tanford, C. *Proc. Natl. Acad. Sci. U.S.A.* **1974**, *71*, 2925–2927.

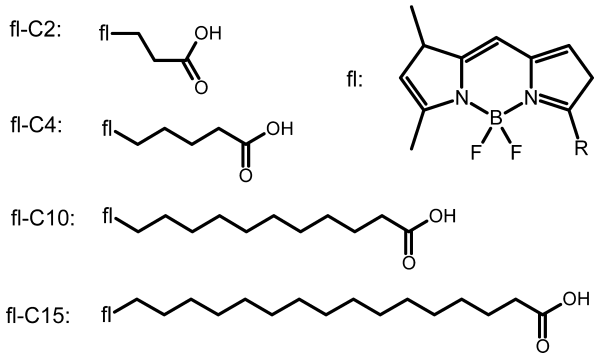

Figure 1. Chemical structures of the molecular probes used in this work.

surfaces.[17] Hydrophobic interactions are critical for the process of protein folding, and long-chain hydrophobic molecules exhibit a phenomenon known as hydrophobic collapse,[18,19] in which they sacrifice the entropy associated with extended conformations in favor of minimizing the solvent-associated surface area by collapsing into a compact globular state. In this manuscript, we examine the effects of molecular conformation by comparing the interfacial behavior of a long-chain amphiphile with shorter-chain homologues.

In a previous paper,[20] we described the capability of total internal reflection fluorescence microscopy (TIRFM) to detect the adsorption and motion of individual surfactant molecules at a solid−liquid interface. We demonstrated that this technique, in contrast to ensemble- or lateral-averaging approaches, represents a powerful way to distinguish mechanisms of mobility at the molecular level and also that interaction energies can be probed by temperature-dependent measurements of molecular motion. In the current work, we have applied this technique to the interfacial motion of the fluorophore-labeled alkanoic acids BODIPY$-(CH_2)_n-$COOH, where $n = 2$, 4, 10, and 15 (abbreviated as fl-C*n*; see Figure 1 for molecular structures), adsorbed at the trimethylsilyl-modified fused silica (TMS-FS)−water interface.

The interaction between these amphiphilic molecules and the methyl-terminated surface is dominated by hydrophobic interactions. Fatty acid surfactants are good model systems for studying hydrophobic interactions in aqueous interfacial systems, in part because of the carboxyl group, which enhances water solubility through hydrogen bonding, and the alkyl tail, which remains largely unsolvated in an aqueous phase.[15] The contrast among the fatty acids used in the experiments described here reflects, in part, the effects of molecular conformation, because fl-C15 is sufficiently long and flexible to adopt a partially folded conformation, while the other molecules are too short to exhibit a compact configuration because of steric hindrance. From a quantitative analysis of molecular trajectories, we have determined that all of these probe molecules alternate between periods where they are virtually immobilized and other periods where they engage in two-dimensional (2D) Brownian motion. The 2D diffusion coefficients were determined quantitatively, and from their temperature dependence, the apparent activation energies and kinetic prefactors were calculated. For the shorter chain lengths, these values increased systematically, as expected; however, fl-C15 exhibited anomalously small values of both parameters. This suggests that fl-C15 may adopt a qualitatively different bound state at the interface (e.g., due to a compact molecular conformation).

Materials and Methods

The substrate preparation followed a careful cleaning procedure in order to minimize the amount of contaminants. A 50 mm diameter fused silica (FS) wafer (MTI Corp.) was cleaned in warm piranha solution for ∼1 h and then subjected to UV−ozone treatment for another ∼40 min. The clean hydrophilic substrate was placed into a Teflon container containing hexamethyldisilazane (HMDS, 99.8% purity, Acros Organics) and positioned ∼15 cm above the liquid to expose its surface to HDMS vapor for ∼48 h. In contrast to solution deposition of self-assembled monolayers (SAMs), this vapor-deposition process ensured that the trimethylsilyl (TMS) layer contained no fluorescent impurities, as confirmed by control TIRFM experiments carried out with pure deionized water (Millipore Milli-Q UV, 18.3 MΩ cm).

Static contact angles of TMS-FS surfaces were measured using a custom-built contact angle goniometer. A liquid drop with a volume of 1 μL was formed at the end of a syringe needle and brought into contact with the surface. Once the needle was removed, the contact angle was measured. Values reported are averages of measurements of at least six drops on three independent samples. Atomic force microscopy (AFM) images were acquired with a Nanoscope MMAFM microscope (Digital Instruments, now Veeco). All of the AFM images were obtained in contact mode using silicon nitride tips. These measurements were made at room temperature (23 ± 1 °C).

Extremely dilute solutions of the probes (Invitrogen, Carlsbad, CA) in water ($\sim 5 \times 10^{-11}$, 6×10^{-12}, 6×10^{-12}, and 3×10^{-12} M for fl-C2, fl-C4, fl-C10, and fl-C15, respectively) were used in these single-molecule experiments; these concentrations were well below the upper solubility limit reported for hexadecanoic acid in water ($\sim 2 \times 10^{-5}$ M).[21] When the solution of interest was introduced into the flow cell, the fluorophores were excited with blue 488 nm light from an Ar ion laser (model 543-A-AO3, Melles-Griot Inc.), and the exposure time was controlled with a Uniblitz shutter (model VMM-D3, Oz Optics Ltd.). A prism-based illumination setup was used to attain the large angle of incidence required for total internal reflection. The blue excitation light and the green emission light of the fluorophores entering the objective were separated with a dichroic mirror (cut-on wavelength ∼505 nm) and a green filter (bandpass ∼515−555 nm). An electron-multiplied CCD camera (model Cascade-II:512, Photometrics Inc.) cooled to −70 °C was used as a photon detector.

Metamorph 6.3 software (Molecular Imaging, Sunnyvale, CA) was used for image and movie acquisition, data processing, and shutter controls. The images acquired were 512 × 512 pixels, and for 60× magnification, the corresponding pixel size was ∼0.078 μm^2. Movies showing single-molecule events (adsorption, desorption, and diffusion) were acquired during continuous exposure to the excitation light; frames were acquired at 2 s time intervals. The raw TIRFM experimental data consisted of movies in which individual molecules appeared as bright diffraction-limited spots. No fluorescent spots were observed in control experiments with pure water. When the fluorescent probe was added, fluorescent spots appeared as a result of adsorption, and the majority of the bright spots moved on the surface. The molecular trajectory coordinates were extracted using the Metamorph 6.3 object-tracking functions.

(16) Oakenfull, D.; Fenwick, D. E. *J. Chem. Soc., Faraday Trans. 1* **1979**, *75*, 636–645.
(17) Christenson, H. K.; Claesson, P. M. *Adv. Colloid Interface Sci.* **2001**, *91*, 391–436.
(18) Miller, T. F.; Vanden-Eijnden, E.; Chandler, D. *Proc. Natl. Acad. Sci. U.S.A.* **2007**, *104*, 14559–14564.
(19) ten Wolde, P. R.; Chandler, D. *Proc. Natl. Acad. Sci. U.S.A.* **2002**, *99*, 6539–6543.
(20) Honciuc, A.; Harant, A. W.; Schwartz, D. K. *Langmuir* **2008**, *24*, 6562–6566.
(21) *CRC Handbook of Chemistry and Physics*, 85th ed.; Lide, D. R., Ed.; CRC Press: Boca Raton, FL, 2004.

Further details concerning the TIRF microscope, flow cell, general procedures, and data-analysis methods used in the current work were presented previously.[20]

Results

TMS-FS surfaces were characterized by contact angle goniometry and AFM. The sessile-drop water contact angle of the TMS-FS substrate was ~96 ± 2°, which is consistent with a hydrophobic surface but smaller than the typical contact angle of ~110° measured on highly organized long-chain SAMs (e.g., octadecylsilanes).[22] AFM images (see Figure S1 in the Supporting Information) showed random, undulating surfaces with an rms roughness of 0.7 nm and no obvious characteristic lateral length scale (features were generally smaller than ~200 nm). These structural characteristics were consistent with those of the underlying FS surface.[20] Lateral force images suggested that the surface was chemically homogeneous on the length scales probed by AFM (i.e., ≥5 nm). Thus, the lower-than-expected contact angle observed for the TMS-FS surfaces may have been due to imperfect lateral organization at the molecular level or to long-range wetting effects arising from interactions between water and the underlying silica surface because the TMS layer was very thin. Previous work has shown that wetting can be affected by interfaces buried less than ~0.5 nm deep.[23]

A total of 87 fl-C2, 118 fl-C4, 221 fl-C10, and 154 fl-C15 independent single-molecule trajectories at the TMS-FS/water interface were recorded and analyzed at temperatures of 14, 19, 25, and 30 °C. It is known that energy due to vibrational relaxation of excited fluorophores is transferred to the water solvent and thermalized within picoseconds.[24−26] Since the probe molecules were excited infrequently during their trajectories, local heating effects were expected to be negligible under the conditions of these experiments. For a convenient graphical depiction of molecular trajectories, we have spliced together the ends of several fl-C15 single molecule tracks acquired at each temperature and presented the result as an effective single-molecule trajectory observed over a long time interval (see Figure 2). While one could justify this procedure in the approximation that the molecular trajectories are ergodic, in fact the analysis below based on squared-displacement distributions was insensitive to splicing. Representative effective trajectories obtained this way (each representing 591 molecular locations over 1183 s) are shown in Figure 2 and provide anecdotal evidence of Brownian behavior and the dependence of the molecular mobility on temperature. The surface area explored by the virtual molecule increased by a factor of ~2 between the lowest and highest temperatures. Furthermore, a careful inspection indicates the coexistence of smaller and larger "steps" intertwined within these trajectories.

In the quantitative analysis of trajectories, it is useful to consider $C(r^2,\tau)$, the integrated (or cumulative) squared displacement distribution (ISDD), as opposed to the raw distribution, because $C(r^2,\tau)$ can be calculated directly from the measured trajectories and does not suffer from binning artifacts

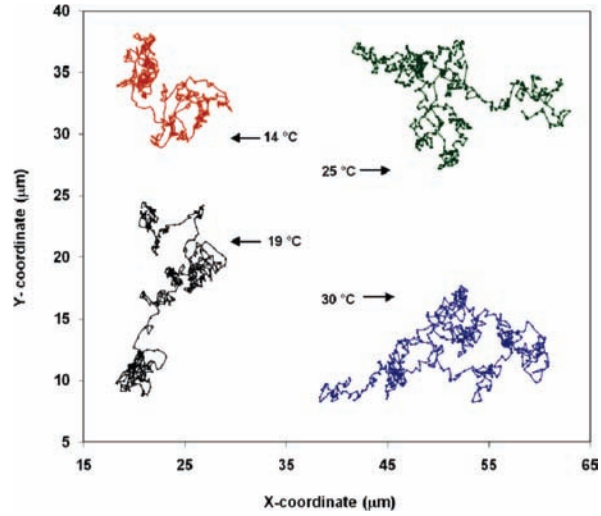

Figure 2. Effective molecular trajectories for fl-C15 obtained by connecting individual molecular trajectories. Each trajectory shown contains 591 data points obtained over 1183 s.

associated with histogram preparation.[27] Intuitively, $C(r^2,\tau)$ is the probability of finding the molecule outside a circle of radius r centered on its original position after a time interval τ. Details of the ISDD calculations were discussed previously.[20] The ISDD curves for the shortest measured time interval, $\tau = 2$ s, are shown in Figure 3.

For simple 2D Brownian diffusion, the expected form of the ISDD is given by $C(r^2,\tau) = \exp(-r^2/4D\tau)$, where D is the diffusion coefficient. Thus, in the semilog representation of Figure 3, where the distribution is plotted against $r^2/4\tau$, the slope of the curve is the reciprocal of an effective diffusion coefficient. In these experiments, however, the data were not in satisfactory agreement with fits to a single exponential. Instead, the data exhibited a crossover from an initial rapid decay to a more gradual decay at larger values of the abscissa. Accordingly, the data were fitted to the following dual-exponential function

$$C(r^2,\tau) = A_1\exp(-r^2/4D_1\tau) + A_2\exp(-r^2/4D_2\tau)$$

which is characteristic of a system with two independent diffusive modes corresponding to different diffusion coefficients.[27] All of the data were adequately described by this function, and the best fits are indicated by the solid lines in Figure 3. Importantly, many trajectories of *individual* molecules exhibited this same type of crossover, indicating that the dual-mode behavior was intrinsic to the molecular motion and not indicative of a mixed molecular population. The parameters corresponding to the best fits are presented in Table 1. The values of D_1, which corresponded to the initial slow mode, were in the range 0.002−0.005 μm^2/s and showed no systematic dependence on chain length or temperature. The values of D_2, on the other hand, were in the range 0.009−0.025 μm^2/s and increased systematically with temperature. A more detailed analysis of this temperature dependence is presented below. On average, A_1 for all chain lengths tended to decrease slightly with increasing temperature, indicating that the probe molecules spent a smaller fraction of time in the slow mode at higher temper-

(22) Peanasky, J.; Schneider, H. M.; Granick, S.; Kessel, C. R. *Langmuir* **1995**, *11*, 953–962.
(23) Bain, C. D.; Whitesides, G. M. *J. Am. Chem. Soc.* **1988**, *110*, 5897–5898.
(24) Lock, A. J.; Woutersen, S.; Bakker, H. J. *J. Phys. Chem. A* **2001**, *105*, 1238–1243.
(25) Ma, H.; Wan, C.; Zewail, A. H. *J. Am. Chem. Soc.* **2006**, *128*, 6338–6340.
(26) Steinel, T.; Asbury, J. B.; Zheng, J.; Fayer, M. D. *J. Phys. Chem. A* **2004**, *108*, 10957–10964.
(27) Hellriegel, C.; Kirstein, J.; Brauchle, C.; Latour, V.; Pigot, T.; Olivier, R.; Lacombe, S.; Brown, R.; Guieu, V.; Payrastre, C.; Izquierdo, A.; Mocho, P. *J. Phys. Chem. B* **2004**, *108*, 14699–14709.

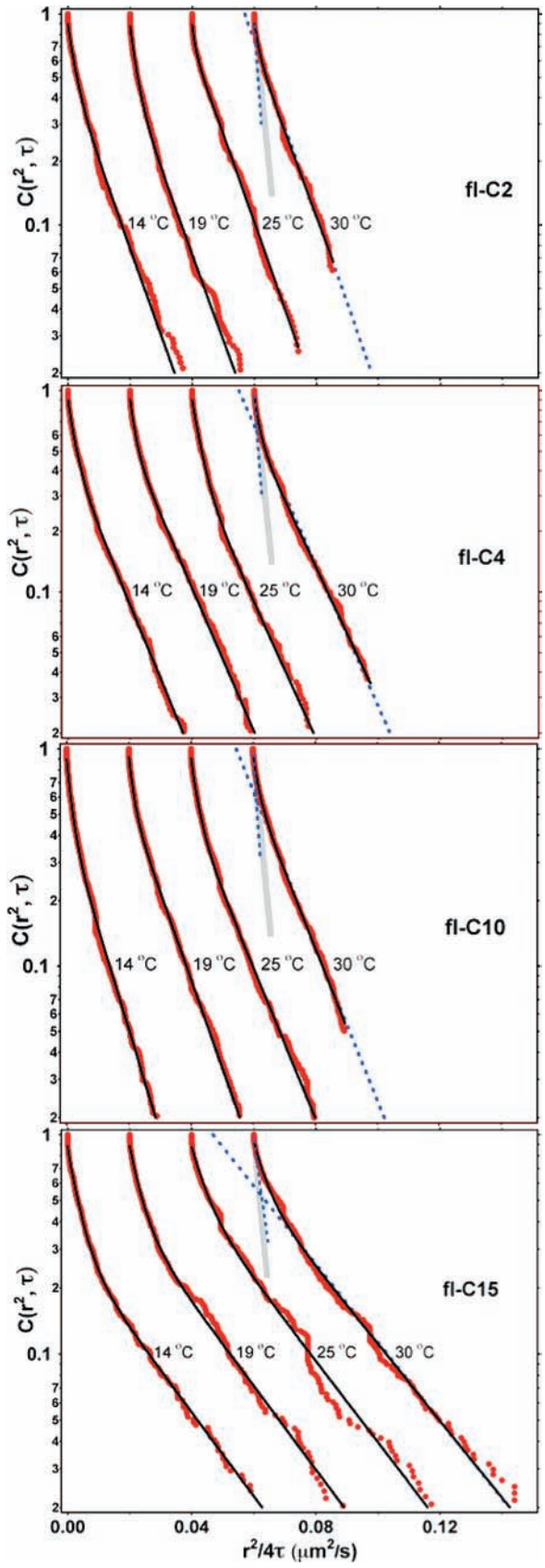

Figure 3. Semilog plots of the integrated squared displacement distributions $C(r^2,\tau)$ with $\tau = 2$ s at the indicated temperatures for (top to bottom) fl-C2, fl-C4, fl-C10, and fl-C15. For clarity, successive distributions have been offset horizontally by 0.02 μm^2/s. For the highest temperatures, the slopes of slow and fast mode distributions are represented by dashed lines, and typical ISSDs for apparent motions of immobilized molecules are represented by thick gray lines.

Table 1. Interfacial Diffusion Parameters as a Function of Temperature (Numbers in Parentheses Represent Uncertainties in the Final Digit)

	T (°C)	D_1 (μm^2/s)	A_1	D_2 (μm^2/s)	A_2
fl-C2	14	0.0031(6)	0.47(6)	0.0106(7)	0.42(6)
	19	0.0027(5)	0.47(5)	0.011(1)	0.40(5)
	25	0.002(1)	0.20(7)	0.0104(8)	0.67(6)
	30	0.003(6)	0.21(4)	0.011(2)	0.66(4)
fl-C4	14	0.0024(6)	0.42(6)	0.0117(7)	0.48(6)
	19	0.0018(5)	0.36(5)	0.0122(6)	0.54(4)
	25	0.0029(8)	0.48(8)	0.0129(5)	0.41(8)
	30	0.0019(9)	0.33(8)	0.013(1)	0.60(7)
fl-C10	14	0.0018(3)	0.45(5)	0.0092(5)	0.45(5)
	19	0.0016(4)	0.36(5)	0.0107(5)	0.56(4)
	25	0.0024(5)	0.42(5)	0.0125(6)	0.49(4)
	30	0.0019(7)	0.30(6)	0.0121(8)	0.63(6)
fl-C15	14	0.0037(3)	0.57(2)	0.0227(7)	0.31(2)
	19	0.0038(5)	0.47(3)	0.023(1)	0.41(3)
	25	0.0046(9)	0.37(4)	0.024(1)	0.51(4)
	30	0.0041(9)	0.37(4)	0.025(1)	0.56(4)

atures. Also, a slight increase in A_1 with increasing chain length was observed. These trends are discussed in greater detail below.

As we previously reported,[20] because of signal-to-noise fluctuations, even immobilized fluorescent probes have some apparent motion; this can be regarded as an effective limit on our experimental resolution. Figure 3 also shows schematic ISDDs for molecules that we believe were immobile on the surface. The apparent diffusion coefficient for these molecules ($\sim$0.003 μm^2/s) is in the same range as the D_1 found from the fitting procedure described above. Thus, it is fair to say that the slow mode observed in the current experiments was too slow for us to accurately resolve and may in fact correspond to temporary immobilization of the probe molecules.

While diffusion data are traditionally presented in the form of mean squared displacement (MSD), such averaged data are insensitive to mechanistic details of molecular motion. An example that is relevant here is the situation where two independent random walks are intertwined (e.g., two step lengths with two different probabilities). In this case, it can be shown that the effective net MSD is simply the average of the two individual MSDs weighted by their respective probabilities. Therefore, analysis of MSD data cannot distinguish a bimodal random walk from a simple random walk whose diffusion coefficient is the average of those for the bimodal one. As shown in Figure 4, the MSD data for fl-C15 (calculated from the spliced trajectories) fail to reveal the complexity of the diffusive mechanism (in the figure, the data at higher temperatures have been offset on the vertical axis for clarity). Effective diffusion coefficients, $D_{\mathrm{eff}}^{(\mathrm{C15})}$, were determined by fitting these data to the relevant equation for 2D diffusion, $\langle r^2\rangle = 4Dt$. The values obtained were 0.010, 0.014, 0.016, and 0.017 μm^2/s at 14, 19, 25, and 30 °C, respectively. These values fall between the relevant values of D_1 and D_2 for fl-C15 (see Table 1) and are in reasonable agreement with the weighted average of the two diffusion coefficients. Since these effective values, which were determined by considering only the mean of the squared displacement distribution, correspond not to a specific molecular process but rather to the weighted average of several processes, an Arrhenius analysis based on these rates would give misleading and physically meaningless information and would fail to reveal the complexity of the diffusive mechanism.

The increase of the D_2 diffusion coefficients with temperature suggested that diffusion at the TMS-FS−water interface is an activated process; the data are presented in Figure 5 in the form

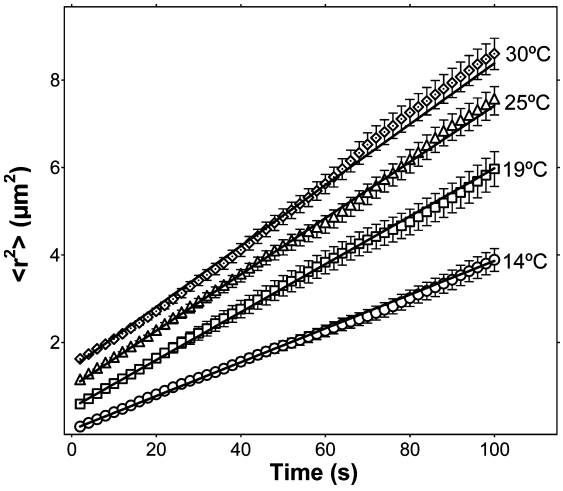

Figure 4. Plots of mean squared displacement vs time for fl-C15 calculated from the effective trajectories at various temperatures. The curves have been offset on the vertical axis for clarity.

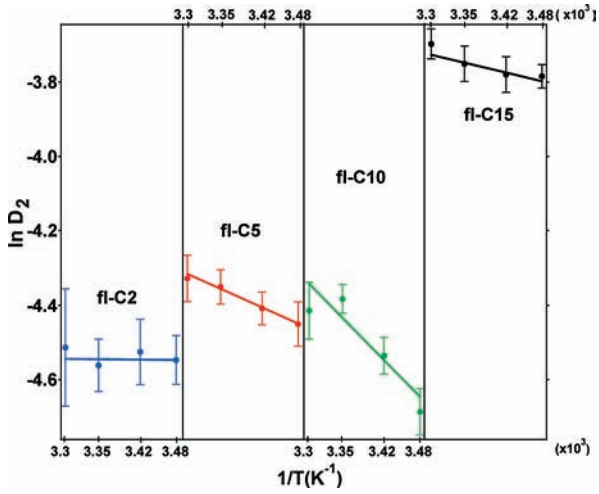

Figure 5. Arrhenius plots for the fast-mode diffusion coefficients (D_2) for fl-C2, fl-C5, fl-C10, and fl-C15.

of Arrhenius plots. Fitting these data to the Arrhenius equation yielded apparent activation energies, E_a, and kinetic prefactors associated with interfacial diffusion for the various probe molecules. According to the standard Arrhenius approach, the natural logarithm of the kinetic prefactor is proportional to the activation entropy, $\Delta S^{\ddagger}$ (i.e., ΔS for going from the reactants to the transition state). Accordingly, the activation energies and ln(prefactor) values are presented in Figure 6 and Table 2.

Both the activation energy and the prefactor exhibited a systematic increase with chain length for fl-C2 through fl-C10, with fl-C15 reversing the trend and displaying anomalously low values (see Figure 6). For the shorter chain lengths, the activation energy increased by 1.5 ± 0.7 kJ/mol per methylene group and the natural logarithm of the prefactor increased by 0.6 ± 0.3 per methylene group.

Discussion

It is instructive to compare our observations with those from previous reports on ensemble-averaged experiments performed on small molecules adsorbed at hydrophobic interfaces. In a fluorescence recovery after photobleaching (FRAP) study of rubrene diffusion on a hydrophobized FS surface in the presence

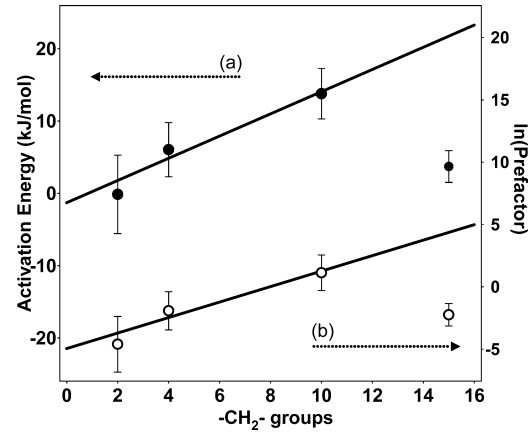

Figure 6. Activation energies and kinetic prefactors for interfacial diffusion as a function of the number of methylene units in the probe molecule. The solid lines represent best fits to the experimental data points corresponding to fl-C2, fl-C4, and fl-C10. The curve fitting yielded the following parameters: (a) slope $= 1.5 \pm 0.7$ kJ/mol per methylene group, intercept $= -1 \pm 5$ kJ/mol; (b) slope $= 0.6 \pm 0.3$ per methylene group, intercept $= -5 \pm 2$.

Table 2. Summary of the Activation Energies and Prefactors Obtained from the Arrhenius Plots in Figure 5

probe	E_a (kJ/mol)	ln(prefactor)
fl-C2	0 ± 5	-5 ± 2
fl-C4	6 ± 4	-2 ± 2
fl-C10	14 ± 4	1 ± 1
fl-C15	4 ± 2	-2 ± 1

of methanol/water,[28] diffusion coefficients at least an order of magnitude larger than those reported here were observed. The mobility depended strongly on the length and coverage of the hydrophobic spacer used to modify the surface and decreased drastically with a reduced methanol fraction in the liquid phase.[29] Other FRAP experiments reported puzzlingly large diffusion coefficients, $\sim 10^2$ μm^2/s,[30] for prodan diffusion on TMS and poly(ethylene glycol) surfaces in contact with nitrogen gas. We believe that these inconsistencies illustrate the difficulties involved in interpreting the results of ensemble-averaging methods (such as FRAP) at interfaces, particularly when competing processes, such as adsorption and desorption of fluorophores at the interface, are present.

As mentioned previously, the presence of two diffusive modes is not explained by the presence of two molecular populations; in many cases, both modes were observed within the same molecular trajectory. A likely explanation for the multiple diffusive modes lies in the possibility that a given probe molecule may associate with the surface in different ways at different times (i.e., there are multiple bound states). Interestingly, the rate at which the molecules sample these different bound states is fast relative to the dissociation rate of the molecule from the surface. The values of diffusion coefficients for the slow mode fell near our lowest detection limit, so one might interpret the slow mode as representing temporary immobilization. It is possible that probe molecules become temporarily trapped at local defect sites or within very small 2D compartments. Figure 7 illustrates the dependence of the

(28) Hansen, R. L.; Harris, J. M. *Anal. Chem.* **1996**, *68*, 2879–2884.
(29) Hansen, R. L.; Harris, J. M. *Anal. Chem.* **1995**, *67*, 492–498.
(30) Heitzman, C. E.; Tu, H. L.; Braun, P. V. *J. Phys. Chem. B* **2004**, *108*, 13764–13770.

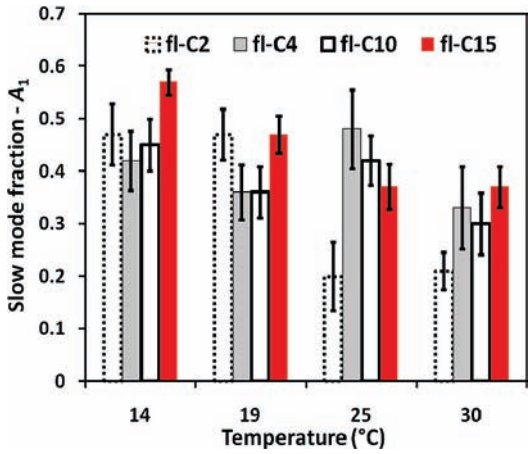

Figure 7. Dependence of the slow-mode fraction A_1 on the temperature and chain length.

A_1 parameter (the slow-mode fraction) on chain length and temperature. Although these data exhibit significant scatter, A_1 generally decreases with increasing temperature. This is consistent with the "trapping" hypothesis, since the greater thermal energy available at higher temperatures would increase the probability of molecular escape from trapped locations. Although there appears to be a slight increase in A_1 for longer chain lengths, this trend is extremely weak and not apparent at all temperatures. The weakness of the dependence on chain length may indicate that the trapping behavior is related to molecular moieties other than the alkyl chain, i.e., the carboxylate or BODIPY groups. These moieties are polar and could potentially interact with regions of the FS surface that are not adequately covered by the hydrocarbon coating.

In the classical picture of surface diffusion, the lateral motion of an adsorbate molecule is considered to involve steps of detachment from a subsurface layer and reattachment to a vicinal adsorption site.[31] For a single molecular step, the activation energy of diffusion is a direct measure of the energy needed to remove a molecule/moiety from the initial adsorption site. The main driving force for fatty acid adsorption at the TMS-FS−water interface is the hydrophobic free energy arising from the reduction of the solvent-accessible surface areas (SASAs) of the solute/adsorbate and the flat surface upon adsorption and displacement of the water layer(s) intercalated between the two.[32] Therefore, we postulate that the free energy of activation for diffusion, $\Delta G^{\ddagger}$, arises from an increase in SASA and partial rehydration of the adsorbate and TMS-FS surfaces upon the departure of the adsorbate from the initial adsorption site into a near-surface layer. For complete rehydration, $\Delta G = \gamma\Delta(\text{SASA})$, where the proportionality constant, γ, is the hydrophobic surface energy density.[33] A number of calculations suggest that ΔG may be a reasonable approximation for $\Delta G^{\ddagger}$, although the free energy of activation may actually be somewhat smaller than the free energy associated with complete hydration if the molecule becomes laterally mobile prior to complete removal from the surface.[34,35]

In this picture, the experimentally observed increase in the activation energy of 1.5 ± 07 kJ/mol per methylene group should be compared with hydrophobic interaction energies from the literature. From experimental solubility measurements of saturated alkanes in water, Reynolds et al.[15] reported an increase in hydrophobic energy associated with the increase of SASA with increasing chain length. They quoted a value of 20−25 cal mol^{-1} A^{-2}, which corresponds to ∼2.5−3.2 kJ/mol per methylene unit since each additional methylene unit contributes ∼30 $Å^2$ to the SASA.[36] Other experimental results are consistent with these values.[15,37,38] Similarly, molecular dynamics simulations[39] of the aggregation of small solutes in water gave a value of 24 cal mol^{-1} A^{-2}. Thus, the increase in the activation energy for 2D diffusion with chain length measured here for fl-C2 through fl-C10 is roughly half of the increase expected for full hydration of the adsorbate. This is consistent with a picture in which the fl-C2, fl-C4, and fl-C10 probe molecules lie in an extended conformation on the surface, with each methylene group interacting with surface hydrophobic groups. The transition state would then involve a small displacement of the adsorbate away from the surface that increases the SASA by an amount insufficient to allow the solute to become completely hydrated. The addition of a methylene unit increases the hydrophobic interaction energy along the general lines of the Traube−Duclaux rule[38] that applies to the transfer of a homologous series of alkanes or fatty acids from an oil to a water phase.

The natural logarithm of the kinetic prefactor is proportional to $\Delta S^{\ddagger}/R$, so the increase by 0.6 per methylene group suggests that $\Delta S^{\ddagger}$ increases by $0.6R$ per methylene group. In the model discussed above, the transition state would thus have increased conformational flexibility compared with the surface-bound state. The number of rotational conformations accessible to an alkyl chain increases by three per added methylene group,[40] so the full rotational entropy of the chain increases by $R \ln 3 \approx 1.1R$ per added methylene unit. The smaller experimental value of $0.6R$ may indicate that the transition state does not have complete rotational flexibility, or it may reflect the reduction of the entropy of solvent (water) molecules in the surroundings.

Notably, the fl-C15 probe molecule did not follow the expected trends of activation energy and entropy with chain length. This suggests that fl-C15 binds to and moves on the hydrophobic surface in a qualitatively different way than the shorter-chain homologues. One possible reason for this could be the greater conformational flexibility of longer-chain molecules. While short-chain alkanes and alkane derivatives are sterically hindered from sampling compact/folded configurations, longer-chain molecules are known to adopt a more collapsed state under certain conditions.

Several computational studies[41−44] have discussed the conformations adopted by *n*-alkanes $CH_3(CH_2)_{n-2}CH_3$ in water and

(31) Dobbs, K. D.; Doren, D. J. *J. Chem. Phys.* **1992**, *97*, 3722–3735.
(32) Israelachvili, J.; Wennerstrom, H. *Nature* **1996**, *379*, 219–225.
(33) Elcock, A. H.; Sept, D.; McCammon, J. A. *J. Phys. Chem. B* **2001**, *105*, 1504–1518.
(34) Choudhury, N.; Pettitt, B. M. *J. Am. Chem. Soc.* **2005**, *127*, 3556–3567.
(35) Latour, R. A.; Rini, C. J. *J. Biomed. Mater. Res.* **2002**, *60*, 564–577.
(36) Gallicchio, E.; Kubo, M. M.; Levy, R. M. *J. Phys. Chem. B* **2000**, *104*, 6271–6285.
(37) Hermann, R. B. *J. Phys. Chem.* **1972**, *76*, 2754–2759.
(38) Lowy, D. A. In *Encyclopedia of Surface and Colloid Science*; 2nd ed.; Somasundaran, P., Ed.; Taylor & Francis: New York, 2006; Vol. 4, p 2544−2556.
(39) Raschke, T. M.; Tsai, J.; Levitt, M. *Proc. Natl. Acad. Sci. U.S.A.* **2001**, *98*, 5965–5969.
(40) Nasipuri, D. In *Stereochemistry of Organic Compounds: Principles and Applications*; Wiley: New York, 1991; p 223.
(41) Athawale, M. V.; Goel, G.; Ghosh, T.; Truskett, T. M.; Garde, S. *Proc. Natl. Acad. Sci. U.S.A.* **2007**, *104*, 733–738.
(42) Mountain, R. D.; Thirumalai, D. *Proc. Natl. Acad. Sci. U.S.A.* **1998**, *95*, 8436–8440.
(43) Mountain, R. D.; Thirumalai, D. *J. Am. Chem. Soc.* **2003**, *125*, 1950–1957.
(44) Wallqvist, A.; Covell, D. G. *Biophys. J.* **1996**, *71*, 600–608.

suggested that short *n*-alkanes are typically found in a linear all-trans conformation[42,44] while longer *n*-alkanes tend to adopt sterically unfavorable "collapsed" or "globular" conformations stabilized by the reduction of their SASA.[41,43] The crossover between short and long in this context is believed to be near $n \approx 17$.[43] Similarly, the hydrophobic free energy was found to scale linearly with chain length for small alkanes, up to the typical lengths where *n*-alkanes adopt globular shapes.[45] These computational studies are supported by solubility data. For short chains, alkane solubility decreases linearly with chain length; however, chains longer than C_{12} have anomalously high solubilities,[46] likely due to globular conformations. Rupture force experiments[47] between *n*-alkane chain pairs in water also showed that the hydrophobic free energy does not scale linearly with chain length; chains longer than hexadecane adopt a globular conformation. Qualitatively similar behavior is expected for *n*-alkyl carboxylic acid surfactants, but the crossover is expected to occur at a longer chain length, e.g., $n \approx 19$.[48] In any case, it is important to note that because of the fluorescent moiety, which is moderately hydrophobic, fl-C15 is likely somewhat more hydrophobic than unlabeled hexadecanoic acid ($n = 15$), and it is not unreasonable to hypothesize that fl-C15 could adopt a compact conformation, particularly near a methylated surface. In fact, a computational study predicted this sort of conformational transition as a function of temperature for a hydrophobic chain near a hydrophobic surface.[49] The low value of the activation energy for fl-C15 is particularly interesting in the context of theories suggesting that the hydrophobic surface energy density, γ, is actually an increasing function of the solute radius of curvature,[50] (i.e., γ was predicted to be smaller for extended conformations than for globular conformations). We hope to be able to test these predictions experimentally in future work.

It is important to note that other molecular models may satisfactorily explain the different interfacial behavior of short- and long-chain amphiphiles. For example, a given bound state (associated with a particular diffusional mode) could be related to the binding of a particular molecular moiety (e.g., BODIPY fluorophore vs alkyl chain). Alternatively, states could be associated with molecular orientation (e.g., lying down vs standing up). While we feel that conformational changes are more likely to explain the discrete nature of the diffusive modes, it is clear that further experiments will continue to shed light on this issue.

These diffusion scenarios demonstrate that molecular mobility at liquid−solid interfaces is significantly more complex than at the solid−vapor interface. In particular, these results are in stark contrast with the conventional picture of *n*-alkanes lying flat and moving rigidly at the single-crystal−vapor interface.[51]

Conclusions

Single-molecule TIRFM observations of surfactant diffusion near a hydrophobic surface have provided quantitative information related to the adsorbate−surface interaction in the presence of water. From a statistical analysis of molecular trajectories, we have established the coexistence of two diffusive regimes for surfactant probe molecules: one where the molecule is nearly immobilized and another with diffusion coefficients that vary systematically with chain length and temperature. The effective activation energies and entropies for the shorter-chain probe molecules scaled linearly with chain length. For the longest chain surfactant, on the other hand, the activation energy and entropy were anomalously low. A mechanistic picture of interfacial diffusion was proposed in which activation barriers to interfacial diffusion are related to the hydrophobic interaction between the surface and the adsorbate molecule and the activation entropy is due to increased conformational freedom in the partially hydrated transition state. The shorter-chain amphiphiles were hypothesized to adopt extended surface conformations in which the entire chains interact with the surface, while it was suggested that the long-chain amphiphile adopts a more compact conformation with minimal surface interaction.

Acknowledgment. The authors acknowledge financial support from U.S. National Science Foundation Award CHE-0349547.

Supporting Information Available: AFM images of TMS-FS surfaces. This material is available free of charge via the Internet at http://pubs.acs.org.

JA900607G

(45) Chandler, D. *Nature* **2005**, *437*, 640–647.
(46) Tsonopoulos, C. *Fluid Phase Equilib.* **1999**, *156*, 21–33.
(47) Ray, C.; Brown, J. R.; Kirkpatrick, A.; Akhremitchev, B. B. *J. Am. Chem. Soc.* **2008**, *130*, 10008–10018.
(48) Smith, R.; Tanford, C. *Proc. Natl. Acad. Sci. U.S.A.* **1973**, *70*, 289–293.
(49) Sengun, Y.; Erzan, A. *J. Phys.: Condens. Matter* **2005**, *17*, S1183–S1194.
(50) Rajamani, S.; Truskett, T. M.; Garde, S. *Proc. Natl. Acad. Sci. U.S.A.* **2005**, *102*, 9475–9480.
(51) Brand, J. L.; Arena, M. V.; Deckert, A. A.; George, S. M. *J. Chem. Phys.* **1990**, *92*, 5136–5143.